JOURNAL OF AIRCRAFT
Vol. 46, No. 6, November–December 2009

Overset Euler/Boundary-Layer Solver with Panel-Based Aerodynamic Modeling for Aeroelastic Applications

P. C. Chen,* Zhichao Zhang,† Ayan Sengupta,† and Danny D. Liu‡
ZONA Technology, Inc., Scottsdale, Arizona 85258

DOI: 10.2514/1.43434

An Euler solver with boundary-layer option, overset/sheared Cartesian mesh, and automated mesh-generation capability has been developed for aeroelastic applications to complex aircraftlike configurations. The automated mesh-generation scheme can automatically generate a block mesh by extending the grid lines from surface meshes to the entire flowfield. In this way, the surface mesh can adopt the paneling definition required by commonly practiced aerodynamic panel methods as input. The overset/sheared-Cartesian-mesh capability allows convenient modeling of very complex configurations, such as an aircraft with external stores, in which the aircraft and stores are modeled by different blocks of meshes. This paper does not describe a novel computational method nor provide new insight into the characteristics of physical problem. Rather, it offers a user-friendly and cost-effective computational methodology that can be readily adopted by industry for rapid aeroelastic applications.

I. Introduction

THE rapid progress of computational fluid dynamics (CFD) methodology in the last decade has shown promising features of its simulated unsteady aerodynamics for flight vehicles. High-level CFD methods such as Reynolds-averaged Navier–Stokes and large-eddy simulation/detached-eddy simulation could indeed capture flow details in their simulated results, serving as research tools for aerodynamic investigations. But whether they could readily become aeroelastic tools for industrial application remains to be seen at present, due to the fact that many aeroelastic problems such as flutter, limit cycle oscillation, and gust loads, among others, require fast turnaround time with limited computing resources. Therefore, the aerospace engineers are accustomed to using panel codes like the doublet lattice method and ZAERO [1,2] as aeroelastic tools. This is because these codes can be readily adopted and run with the aerodynamic paneling scheme, which is by far simpler than the grid-generation procedure required by the CFD methods. Perhaps the only drawback of these codes is that they are largely based on potential-flow methods, lacking flow nonlinearity and rotationality due to shock waves that occurr in the high-speed flight regimes. Therefore, there has been large demand in recent years from the aerospace industry to acquire higher-level CFD methods that can accurately capture such types of flow nonlinearity and be computationally efficient for expedient aeroelastic applications. In addition, the acquired CFD method should be ideally grid-generation free for the user; its input format would be best to adopt that of the panel codes, hence relieving the grid-generation burden of the user to readily perform aeroelastic analysis. These considerations thus motivated the recent development of an unsteady Euler-equations-based solver.

By largely improving the algorithms of XTRAN3S [3], Batina [4] developed an unsteady transonic flow solver called CAPTSD which solves the unsteady transonic small-disturbance equation (TSDE) on a "sheared" Cartesian mesh. The purpose of the sheared Cartesian mesh is to accommodate the sweep angle of the horizontal lifting surfaces so that they can be fitted into such a sheared Cartesian mesh. CAPTSD was further improved by Edwards [5] in coupling the inviscid potential flow solution with a boundary-layer method to include the viscous effects. Batina [4] has further demonstrated the computational efficiency and ease in mesh generation of the CAPTSD code in many transonic aeroelastic problems. However, because of the TSDE assumption, the CAPTSD code can neither model the entropy gradients for strong shock nor capture the vorticity correctly, hence limiting its applicability for weak shocks. Batina later advanced the CAPTSD with a consistent TSDE formulation called ASP3-D [6], in which the flow vorticity, shock predictions, and leading-edge behavior, among other features, were largely improved. Unfortunately, validation effort has been lacking to justify its potential for a full-fledged aeroelastic tool. Thus, following the CAPTSD formulation as an aeroelastic tool guideline, one naturally looks for a higher-level sheared-Cartesian-based CFD method that could overcome the shortcomings of a TSDE approach.

Gao et al. [7] and Zhang et al. [8] have developed an Euler solver, called the CartEuler code, to replace the potential flow solver in the CAPTSD code. The CartEuler code solves the Euler equations on a similar sheared Cartesian mesh and couples the boundary-layer method adopted from CAPTSD for viscous flow solutions. Zhang et al. approximated the full Euler boundary condition by its first-order expansion about the mean plane of the lifting surfaces, which allows the thickness distribution of the surface be incorporated in the Cartesian mesh formulation. For unsteady aerodynamic computation, CartEuler employs the so-called transpiration boundary condition [9] to account for the structural displacements/modes on the nonmoving Cartesian mesh. The CartEuler approach offers an appropriate balance between the complete modeling of flow physics and the computational efficiency, and clearly shows a promising potential for efficient aeroelastic applications in an industrial design environment. For a wing–body–tail configuration, however, one still needs a rather laborious mesh-generation effort with CartEuler, in which all components in the configuration must be fitted into a single block of sheared Cartesian mesh. For an aircraft with underwing stores, it is apparent that the sheared-Cartesian-mesh approach is inadequate to model all components of this complex configuration with a single block of mesh. To resolve these technical issues, we have substantially developed a computational framework on the CartEuler flow solver with an automated mesh-generation scheme and an overset/sheared Cartesian mesh that can largely reduce the mesh-generation effort for aeroelastic analyses of the aircraftlike configurations. The resulting computer code is called the ZEUS code.

II. ZEUS Code

ZEUS is a ZONA Euler unsteady aerodynamic solver that integrates the essential disciplines required for aeroelastic design/

Presented at the 50th AIAA/ASME/ASCE/AHS/ASC Structures, Structural Dynamics, and Materials Conference, Palm Springs, CA, 4–7 May 2009; received 26 January 2009; revision received 26 May 2009; accepted for publication 2 June 2009.

*Vice President. Associate Fellow AIAA.
†Research Engineer.
‡President. Fellow AIAA.

- ZONE 1: Left launcher
- ZONE 2: Outboard left wing
- ZONE 3: Inboard left wing and outboard left horizontal tail
- ZONE 4: Outboard left strake and inboard left horizontal tail
- ZONE 5: Inboard left strake
- ZONE 6: Fuselage
- ZONE 7: Inboard right strake
- ZONE 8: Outboard right strake and inboard right horizontal tail
- ZONE 9: Inboard right wing and outboard right horizontal tail
- ZONE 10: Outboard right wing
- ZONE 11: Right launcher

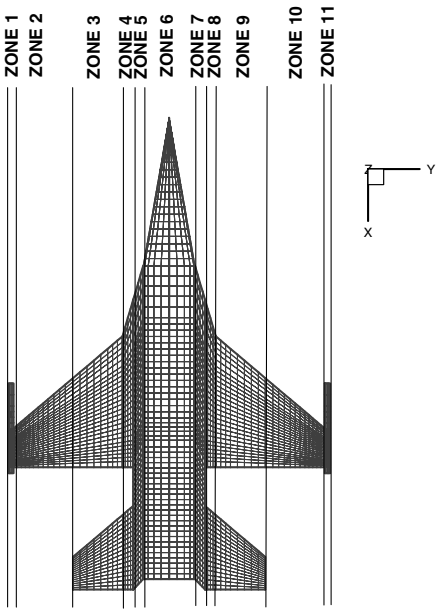

Fig. 1 *Y*-zone technique for a fuselage–strake–wing–tip launcher-horizontal-tail configuration.

analysis. It uses the CartEuler flow solver with a boundary-layer option to include viscous effects as the underlying aerodynamic force generator coupled with structural finite element modal solution to solve various aeroelastic problems, such as flutter, maneuver loads, store ejection loads, gust loads, and static aeroelastic/trim analysis.

ZEUS uses the bulk data input format that is very similar to that of Nastran and ZAERO. In fact, the majority of the input bulk data cards of ZEUS are identical to those of ZAERO. The major difference in input between ZEUS and ZAERO is the mesh generation, because ZEUS requires the mesh of the entire flowfield domain whereas ZAERO only needs the surface mesh. However, ZEUS is equipped with an automated mesh-generation scheme that can automatically generate a flowfield mesh by extending the mesh from the surface mesh. In addition, ZEUS has an overset mesh capability to handle very complex aircraftlike configurations such as a complete aircraft with external stores.

The transferal of displacements and aerodynamic forces between the structural and aerodynamic grids in ZEUS is accomplished by a 3-D spline approach. This 3-D spline approach consists of four spline methods that jointly assemble a spline matrix. These four spline methods include 1) thin plate spline [10], 2) infinite plate spine [11], 3) beam spline [12], and 4) rigid body attachment methods. The spline matrix can transfer the x, y, and z displacements and slopes from the structural grids to all aerodynamic grids as well as the forces at the structural grids to the aerodynamic grids.

For the transient response analysis, the Euler solver is coupled with a state-space equation that involves the generalized mass, damping, and stiffness of the structures. At each time step, the state-space solution is first solved, then the solution of the generalized coordinates are applied to the boundary condition of the Euler equations to compute the aerodynamic forces for the next time step, providing a closely coupled aeroelastic simulation for nonlinear aeroelastic analysis.

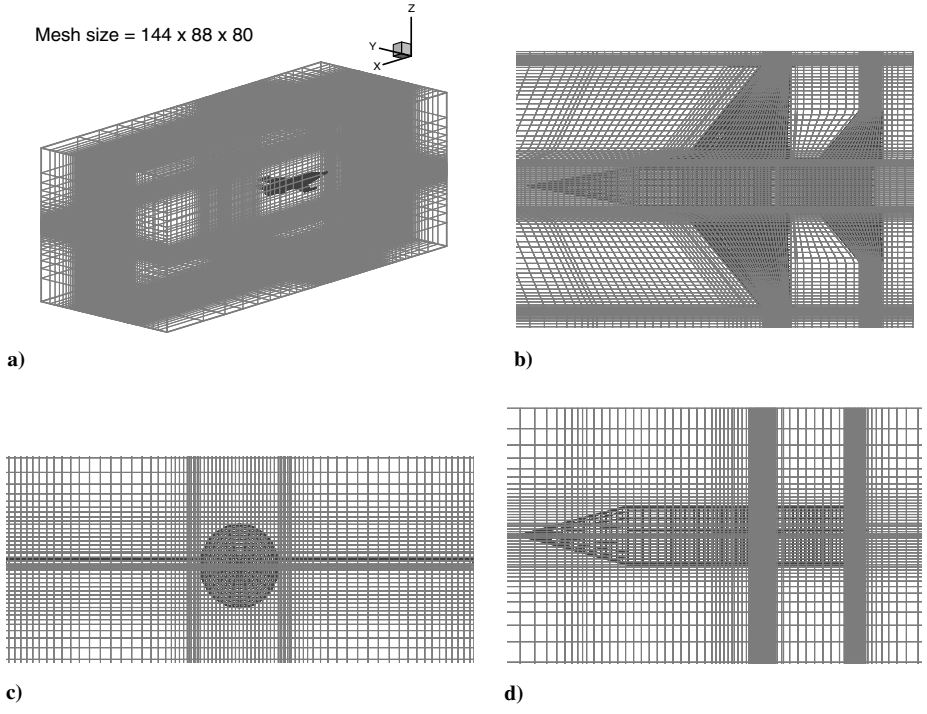

Fig. 2 Automatic generated mesh for a fuselage–strake–wing–tip launcher-horizontal-tail configuration.

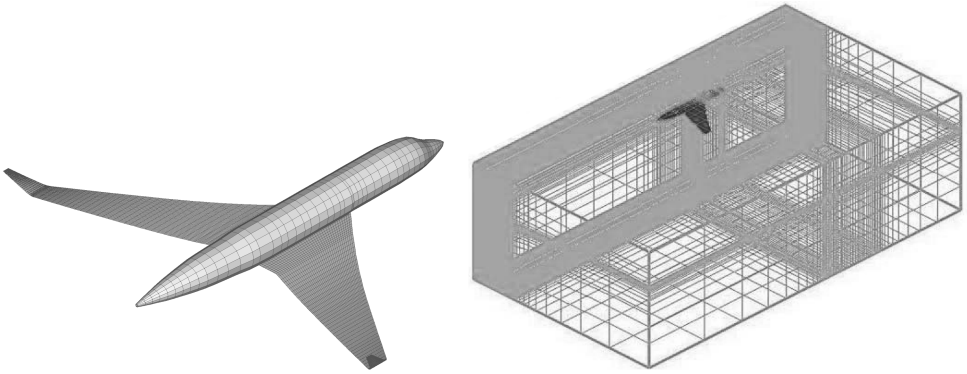

a) ZAERO panel model b) 3-D view of the mesh

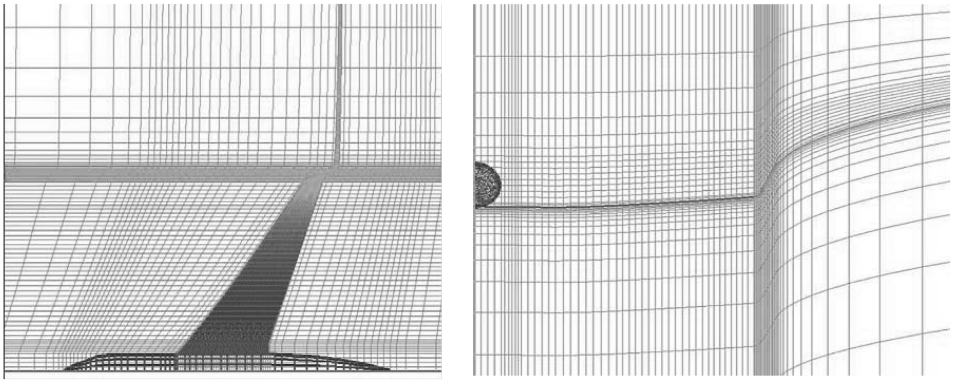

c) Sheared gridlines on X-Y plane d) Sheared gridlines on Y-Z plane

Fig. 3 Sheared mesh of a wing–body configuration with winglet.

ZEUS can also generate the frequency-domain generalized aerodynamic forces that can be readily adopted by the flutter solution technique, such as the *g* method [13] for frequency-domain flutter solution. The frequency-domain generalized aerodynamic forces are computed using a series of decayed sinusoidal functions corresponding to the frequencies of interest to excite a given mode shape. The frequency-domain generalized aerodynamic forces are then obtained by transforming the time-domain transfer function to the frequency domain using Fourier transform.

For statistic aeroelastic/trim analysis, ZEUS computes the aerodynamic stability derivatives of the trim variables using a pseudo-time-domain aerodynamic computation. These trim variables include angle of attack (AoA), side slip, control surface deflections, and pitch, roll, and yaw rates that are provided to a linear trim module to search for the nonlinear trim solution in an iterative manner. At each iteration, the aerodynamic stability derivatives are recomputed based on the last trim condition. The trim solution is converged when the variation of the trim-variable solutions between two iterations becomes sufficiently small.

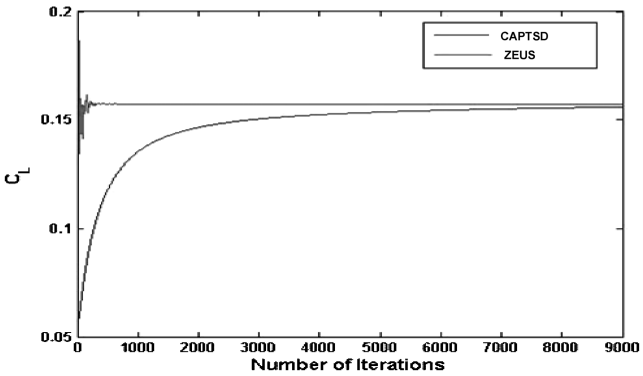

Fig. 4 Convergence study for a fighter configuration at $M = 0.17$ and AoA = 2.2 deg.

III. Automated Mesh Generation

The purpose of the automated mesh-generation capability in ZEUS is to automate the manual volume mesh-generation effort for the aircraftlike configurations. This is accomplished by a ZAERO-to-ZEUS model converter incorporated in ZEUS that adopts the surface mesh of ZAERO, but with much more refined surface mesh than that normally required by the panel method, as input and automatically generates a single block of volume mesh. In this block of mesh, a set of the components of the aircraft, such as fuselage, strake, wing, and horizontal tail, can be fitted. Other components such as the underwing stores can be modeled by additional blocks of mesh. Communication among different blocks of mesh is accomplished by the overset mesh scheme. The volume mesh consists of orthogonal grid lines on the *Y–Z* and *X–Y* planes; that is, the vertical and horizontal grid lines are perpendicular with each other. The grid lines on the *X–Y* plane and the *Y–Z* plane can be further sheared to accommodate the sweep angle of the leading and trailing edges and the dihedral angle, respectively, of the lifting surfaces. This sheared mesh on the *X–Y* plane is automatically generated by a *Y*-zone technique. The *Y*-zone technique projects all components such as the fuselage, strake, wing, tip launcher, and horizontal tail such as those shown in Fig. 1 on the *X–Y* plane. On this *X–Y* plane, all components are divided into

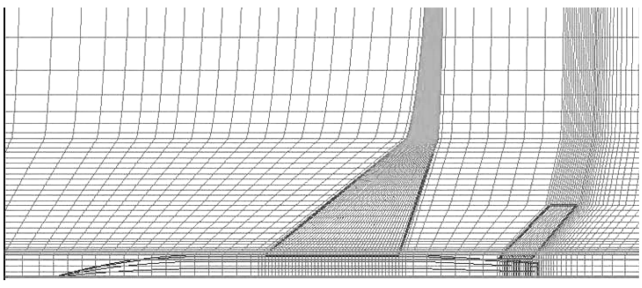

Fig. 5 Mesh on the *X–Y* plane of the L56A18 wind-tunnel model.

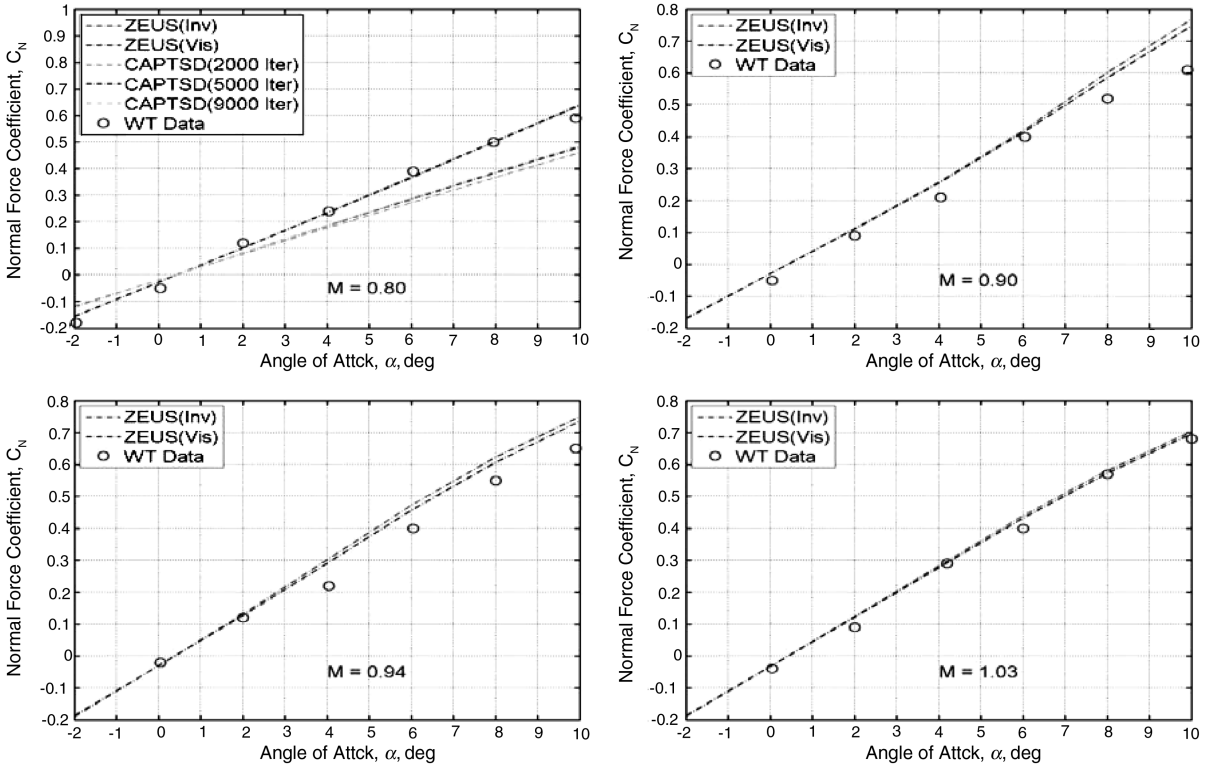

Fig. 6 Normal force coefficients vs angles of attack of the L56A18 wind-tunnel model at $M = 0.8$, 0.9, 0.94, and 1.03.

several spanwise zones, called the Y zones. Within each Y zone, numerous fictitious spanwise lines are first generated whose slopes start from that of the leading and trailing edges of those components in the same Y zone and gradually decrease to zero as they move downstream and upstream. Then, a line tracing method is activated where each spanwise line of the surface mesh traces the fictitious spanwise line across all Y zones, thereby connecting all the spanwise lines. The final step of the Y-zone technique is to check duplicate spanwise lines using a small tolerance; within this tolerance, only one spanwise line is kept.

To extend the spanwise lines to the far field, a cubic spline technique with two slope constraints is used. The lines leaving the rightmost or the leftmost point of the surface mesh should have consistent slope with that of the outer components. Also, they must be perpendicular to the right and the left far-field boundaries when they reach them. The resulting automatic generated mesh for a

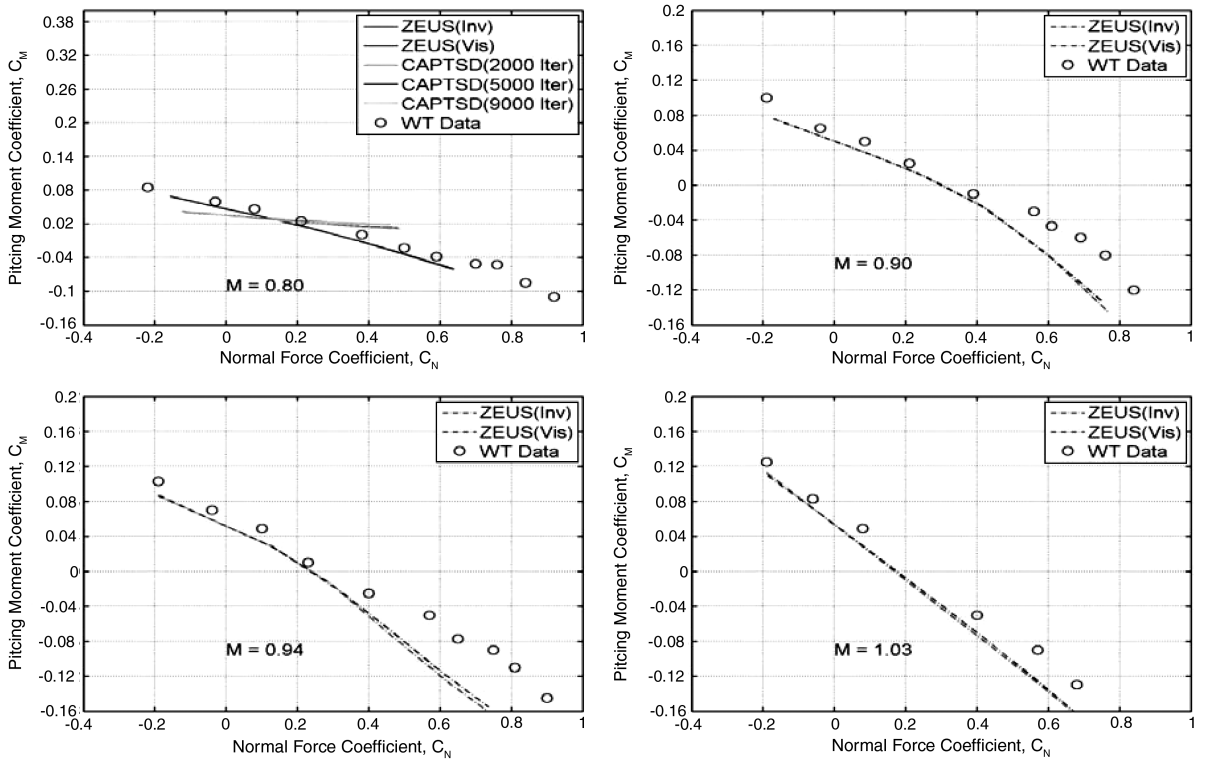

Fig. 7 Pitch moment coefficients vs angles of attack of the L56A18 wind-tunnel model at $M = 0.8$, 0.9, 0.94, and 1.03.

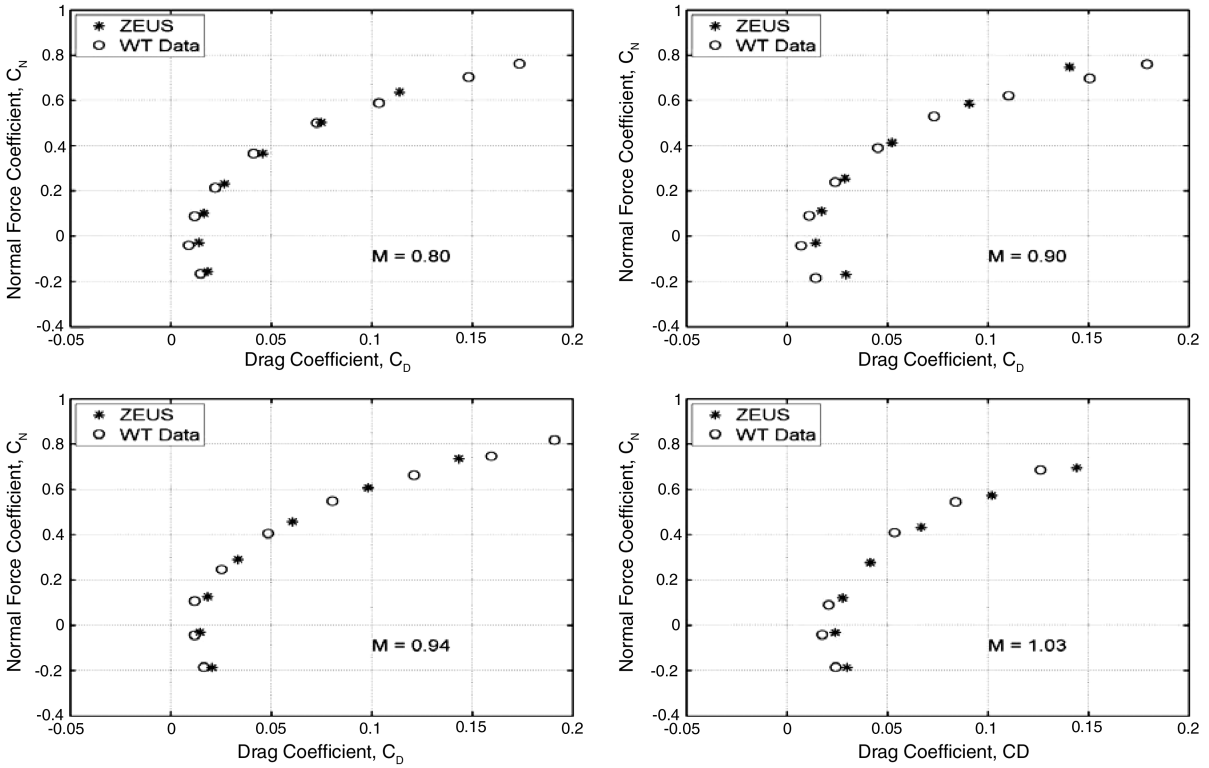

Fig. 8 Drag polars of the L56A18 wind-tunnel model at $M = 0.8, 0.9, 0.94$, and 1.03.

fuselage-strake-wing-tip launcher-horizontal-tail configuration is shown in Fig. 2. It should be noted that the boundary condition of the fuselage is applied on a boxlike prismatic surface that embodies the actual surface of the fuselage. Boppe [14] suggests that a correction parameter using a slender body theory can be derived to account for the spatial difference between the prismatic and the actual surfaces. It is this correction parameter that enables the bodylike components such as fuselage and stores to be modeled by a Cartesian mesh.

The Y-zone technique can be also applied to shear the grid lines on the Y–Z plane to accommodate the dihedral angle of the lifting surfaces. Shown in Fig. 3a is the ZAERO panel model of a wing–body configuration with a winglet. Because of the winglet, the grid lines on the Y–Z plane are sheared by the Y-zone technique so that the grid lines above and below the winglet are nearly parallel to the winglet mean surface. Applying the Y-zone technique to the grid lines on the X–Y plane and the Y–Z plane, the resulting sheared grid lines are shown in Figs. 3c and 3d, respectively.

The automated mesh-generation capability greatly reduces the mesh-generation effort and allows a rapid change of grid size for an optimum mesh density. In fact, the majority of the ZEUS input format is identical to that of ZAERO, so that only the surface mesh defined by the ZAERO panel model but with much more refined mesh is required for input; rendering ZEUS a user-friendly computational aeroelastic tool.

IV. Overset Mesh Scheme

For a complex configuration, it sometimes is very difficult to fit all components of the configuration into a single-block mesh. In this situation, the overset mesh scheme can be employed to fit the components into multiple blocks of mesh. For instance, for a wing with an underwing store configuration, the wing can be fitted into a block of mesh, whereas the store can be fitted into another block of mesh. The communication of the flow solution among blocks can be achieved by interpolating the flow solution in the overlapped-mesh region.

The overset mesh scheme, or called the Chimera scheme [15–17], is a matured technology widely used by the CFD community to model complex configurations using structured grids. Because the ZEUS mesh is structured, the Chimera scheme can be applied directly. The overset mesh scheme incorporated in ZEUS consists of three steps: 1) hole cutting, 2) donor cell search, and 3) finding the interpolation factors. Hole cutting is also referred to as blanking, which nullifies the contribution from those nonphysical points in the overlapping region. The donor cell search finds the cells for the Chimera boundary points in the neighboring body meshes. The flow solutions are interpolated from those donor cells onto the Chimera boundary points. This interpolation is achieved using interpolation factors based on the topology of the meshes in the overlapping regions. Solution convergence within each time step is achieved by subiteration.

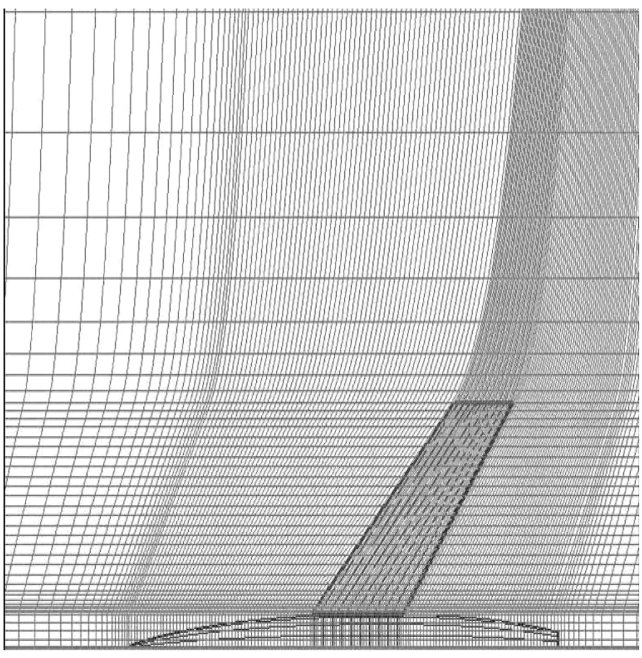

Fig. 9 Mesh on the X–Y plane of the L51F07 configuration.

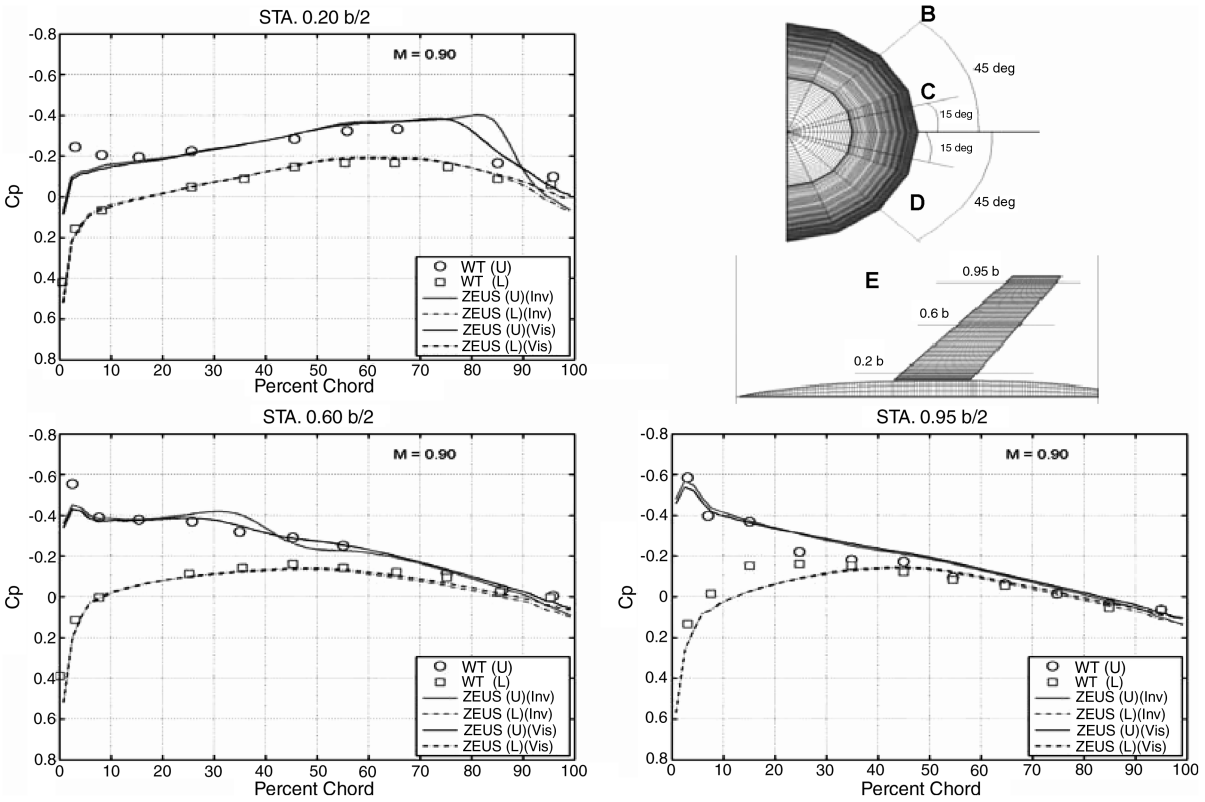

Fig. 10 C_p distribution along three spanwise stations of the L51F07 configuration at $M = 0.9$ and AoA $= 2$ deg.

V. Convergence Study of Steady Aerodynamics on a Fighter Configuration

It is generally believed that the computational time to achieve a converged solution of the Euler solver is longer than that of a potential flow solver. However, our finding showed that this is not the case for ZEUS when it is compared with CAPTSD. Figure 4 presents the convergence of the lift coefficient C_L at $M = 0.7$ and angle of attack AoA $= 2$ deg computed by ZEUS and CAPTSD of a fighter

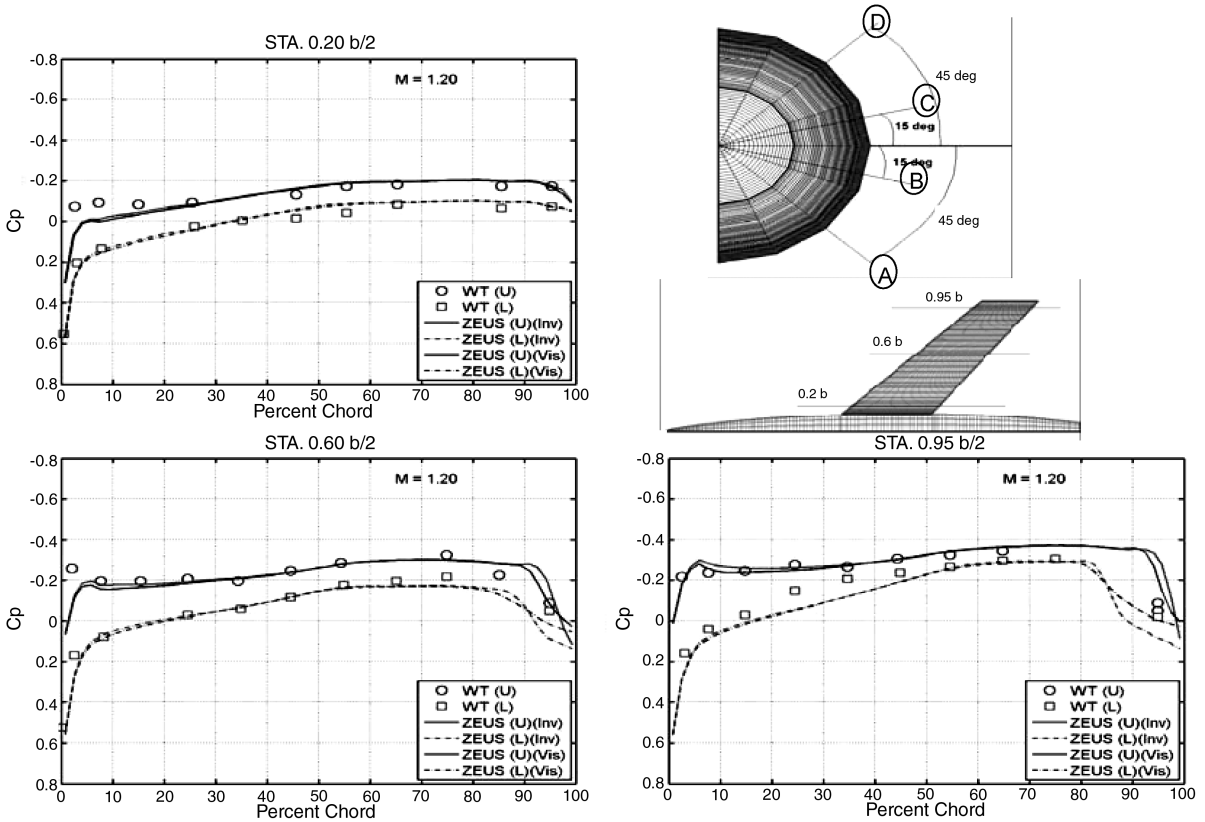

Fig. 11 C_p distribution along three spanwise stations of the L51F07 configuration at $M = 1.2$ and AoA $= 2$ deg.

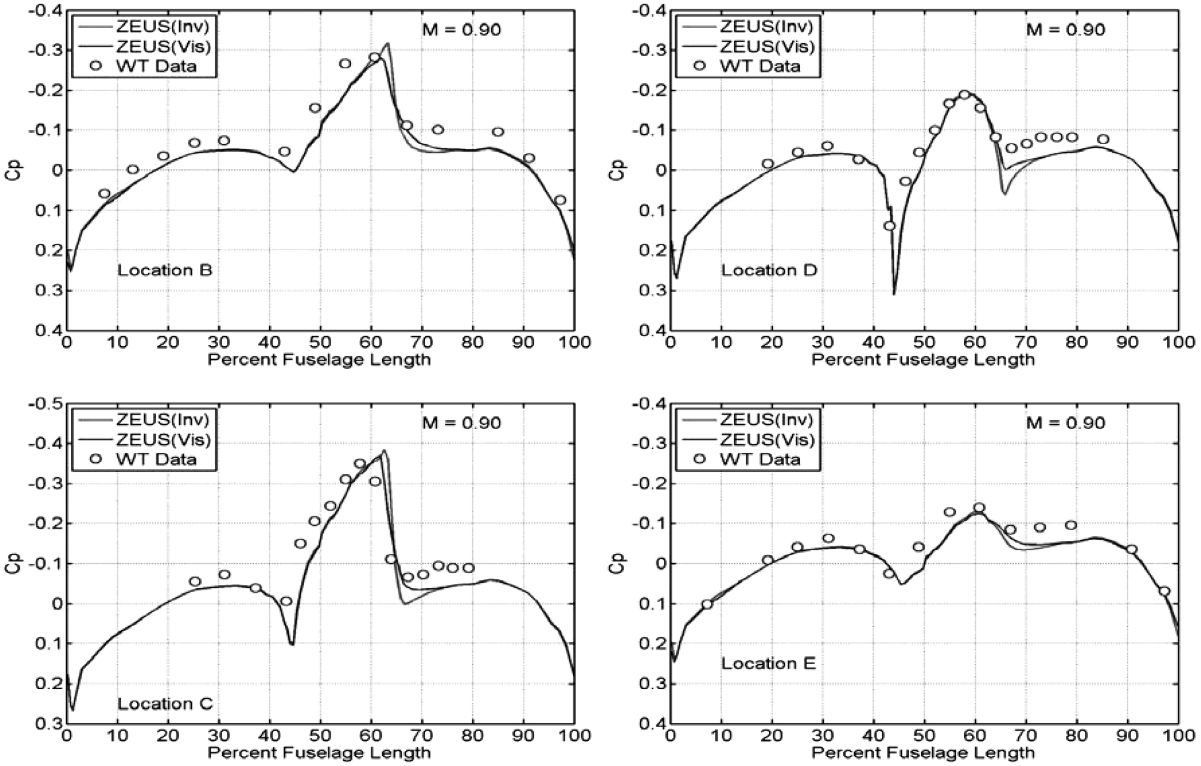

Fig. 12 C_p along the body of the L51F07 configuration at $M = 0.9$ and AoA $= 2$ deg.

configuration shown in Fig. 2. It can be seen that the ZEUS solution converges after 700 iterations but the CAPTSD solution requires 9000 iterations to achieve a nearly converged solution.

The CPU time per iteration of CAPTSD and ZEUS is 0.472 and 2.815 s, respectively. Thus, the total CPU time for a converged solution of CAPTSD (after 9000 iterations) requires 4247 s, whereas the time for ZEUS (after 700 iterations) is only 1970 s. In this case, ZEUS indeed converges much faster than CAPTSD.

VI. Lift, Moment, and Drag Coefficients of the L56A18 Wind-Tunnel Model

The L56A18 wind-tunnel model [18] is a wing–body–tail configuration for which the mesh on the X–Y plane generated by the automated mesh-generation scheme is shown in Fig. 5. The lifts, pitch moments, and drag polars at Mach numbers $M = 0.8, 0.9, 0.94$, and 1.03 computed by ZEUS and CAPTSD, as well as the compar-

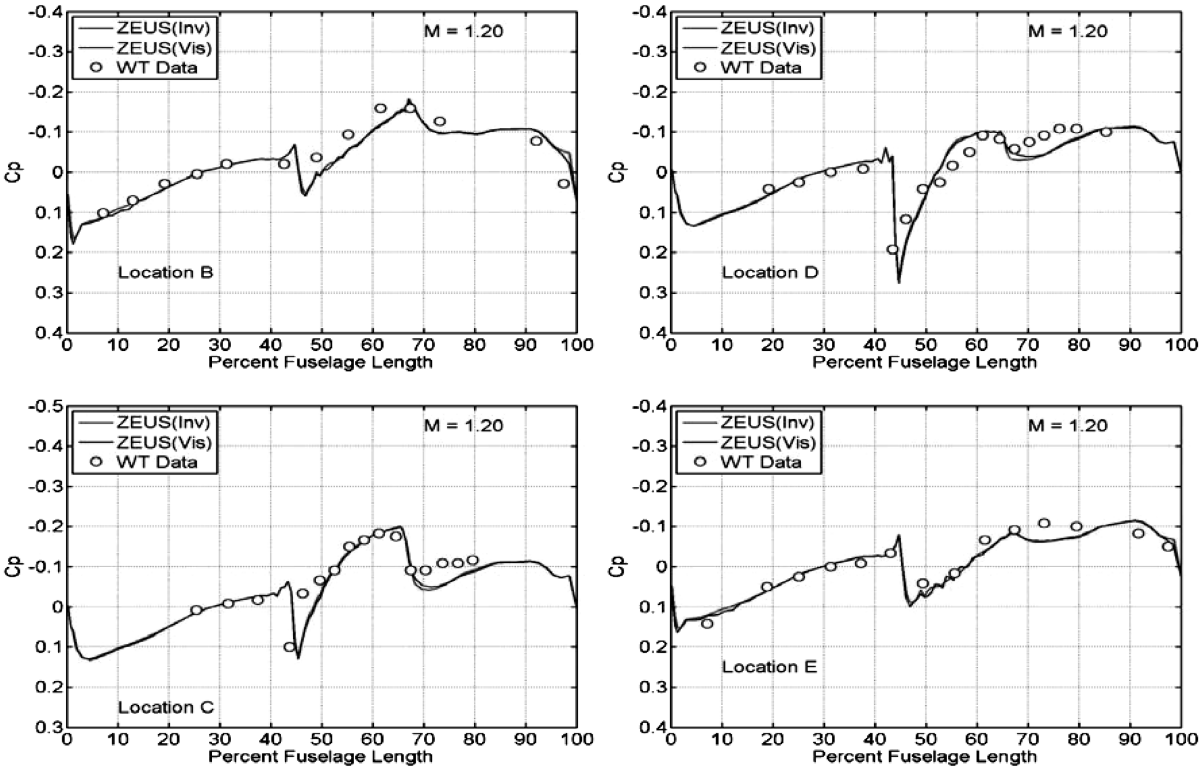

Fig. 13 C_p distribution along the body of the L51F07 configuration at $M = 1.2$ and AoA $= 2$ deg.

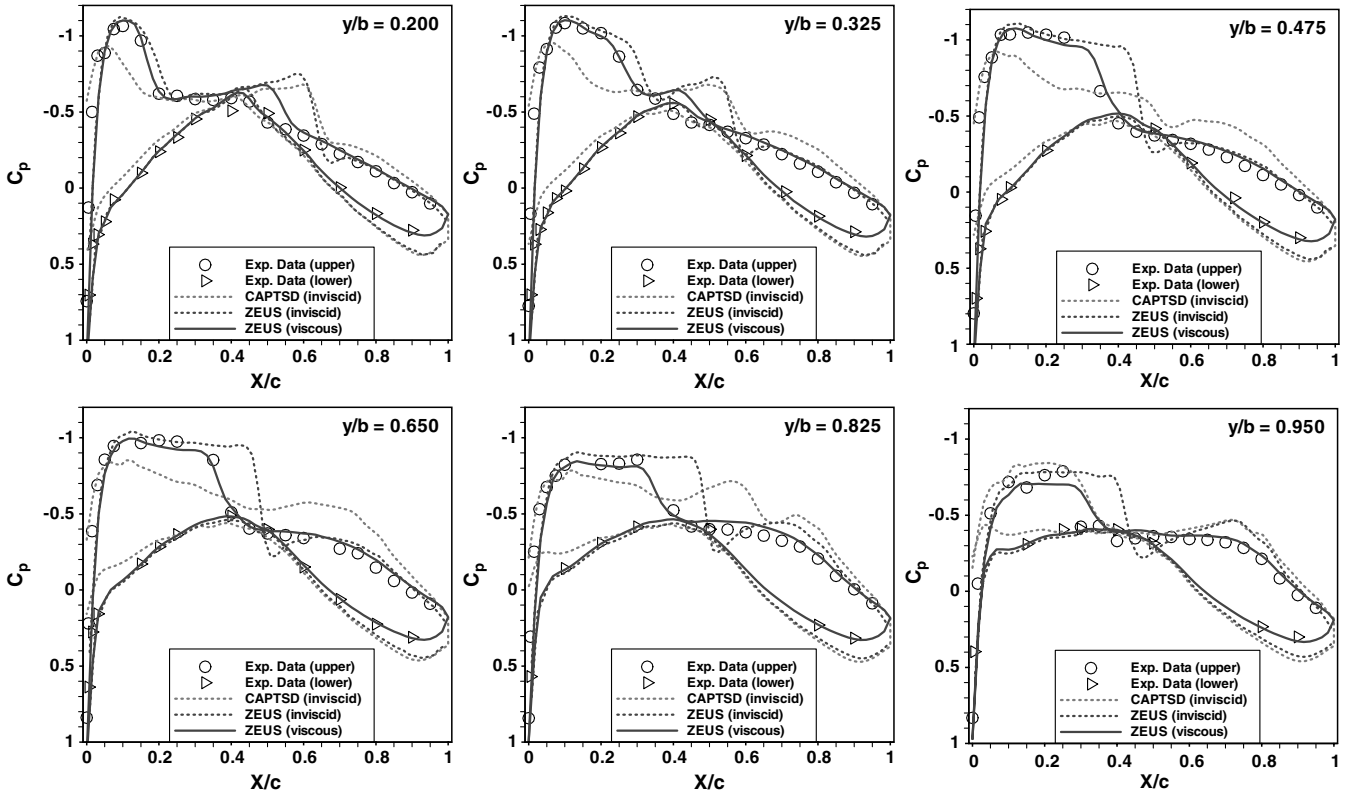

Fig. 14 Steady C_p on the LANN wing at $M = 0.822$ and AoA $= 0.6$ deg.

ison with wind-tunnel data, are shown in Figs. 6–8, respectively. The converged solution of ZEUS at all flow conditions are obtained after 700 iterations. It can be seen that, compared to the wind-tunnel data, the viscous solutions of ZEUS (with boundary-layer option) provides a slight improvement over the inviscid solutions (without boundary-layer option) but only at high-angle-of-attack conditions. Overall, the ZEUS solutions correlate well with the wind-tunnel data mostly at the low-angle-of-attack conditions. On the other hand, the CAPTSD solutions converge slowly from 2000 to 9000 iterations and correlate poorly with the wind-tunnel data, even after 9000 iterations. The better correlation of ZEUS than that of CAPTSD with increased angle of attack is expected in that the equations of the former are of

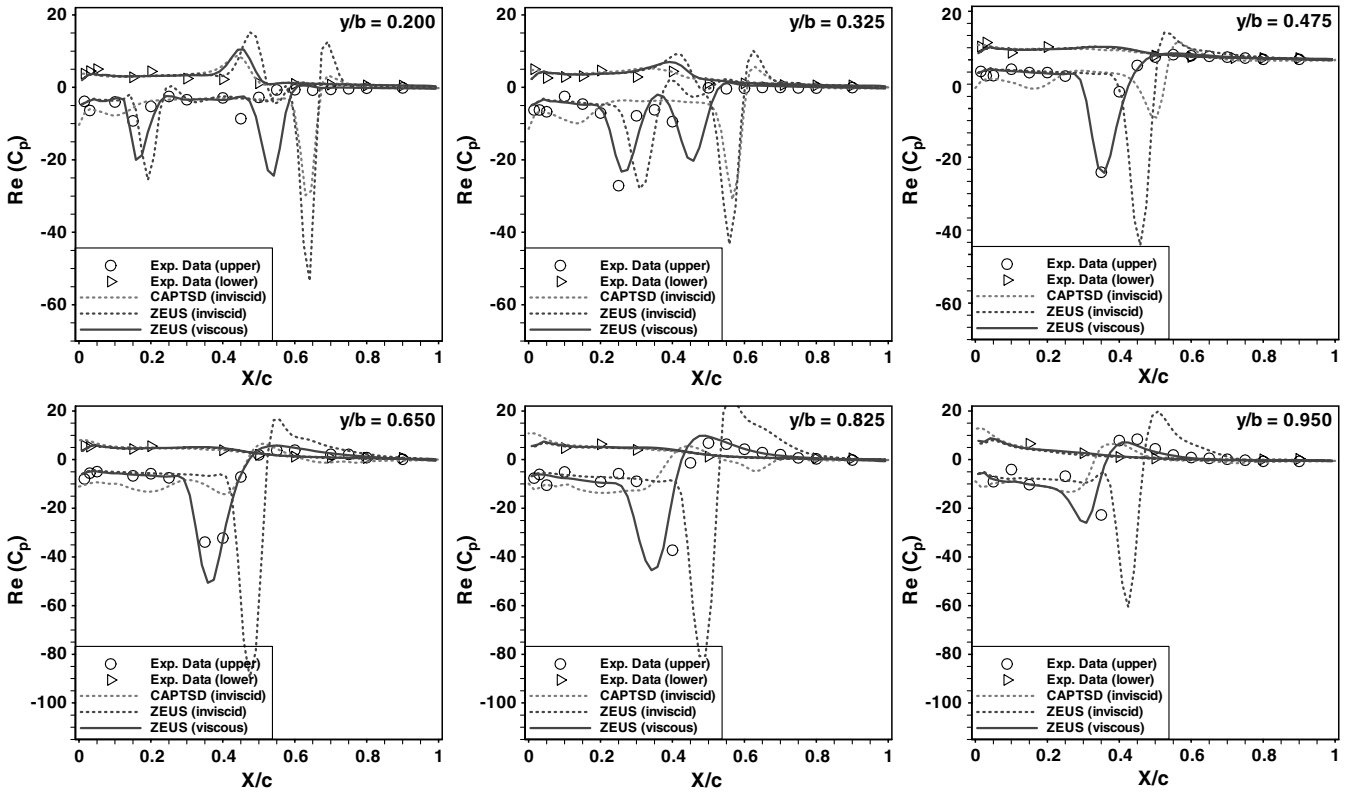

Fig. 15 Real part of unsteady C_p on the LANN wing pitching about its 62.1% root chord at $k = 0.102$ and at $M = 0.822$ and AoA $= 0.6$ deg.

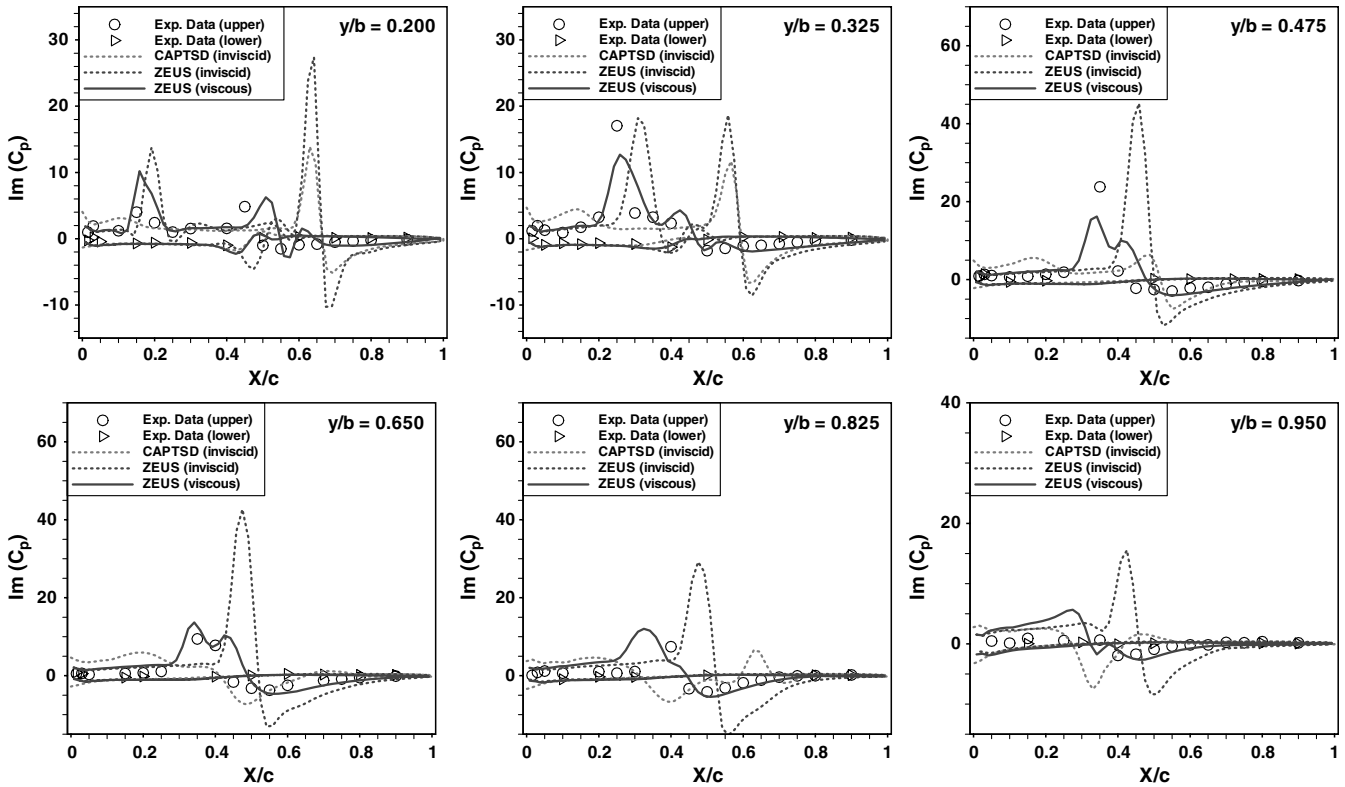

Fig. 16 Imaginary part of unsteady C_p on the LANN wing pitching about its 62.1% root chord at $k = 0.102$ and at $M = 0.822$ and AoA $= 0.6$ deg.

Euler level and unperturbed, whereas that of the latter are based on a perturbed potential flow formulation TSDE, which is known for its limited validity in the angle-of-attack range.

VII. Steady Pressure Coefficients of the Wing–Body L51F07 Configuration

The L51F07 configuration is a wing–body wind-tunnel model for the measurement of its steady pressure coefficient C_p distributions at various flow conditions [19]. The mesh for this case, generated by the automated mesh-generation scheme, is shown in Fig. 9.

The C_p distributions computed by ZEUS and measured by the wind-tunnel test at span stations $0.2\frac{b}{2}$, $0.6\frac{b}{2}$, and $0.95\frac{b}{2}$ of the wing at AoA $= 2$ deg and at $M = 0.9$ and 1.2 are presented in Figs. 10 and 11, respectively, where both ZEUS viscous and inviscid solutions are shown. As expected, the viscous solution significantly improves the shock locations over that of the inviscid solution. Overall, the ZEUS viscous solutions correlate very well with the wind-tunnel data, except the ZEUS solution slightly underpredicts the pressure jump near the leading edge. This is probably due to the rapid change of wing thickness at the leading edge where the approximate boundary condition of ZEUS loses its accuracy and causes such an underprediction.

Because ZEUS employs an approximate boundary condition on a boxlike prismatic surface rather than on the actual surface of the bodies, one might have thought that the C_p distribution on the body could lose accuracy. To show that this is not the case for ZEUS, and the approximate boundary condition for the bodies actually works surprisingly well, we correlated the ZEUS predicted C_p distribution with the wind-tunnel data along the body at four circumferential angles of -45, -15, 15, and 45 deg. This is shown in Figs. 12 and 13 for $M = 0.9$, and AoA $= 2$ deg, as well as for $M = 1.2$ and AoA $=$ 2 deg conditions, respectively. It can be seen that the ZEUS solutions on the body agree well with the wind-tunnel data, and the wing–body interference, especially near the wing–body juncture, is well predicted by ZEUS, demonstrating the validity of the approximate boundary condition of the bodies.

VIII. Unsteady Pressures on the LANN Wing

To show the accuracy of the ZEUS approximate boundary condition on the mean plane of the lifting surface, even for thick wing configurations, the measured unsteady C_p on the LANN wing pitching about 62.1% of its root chord at reduced frequency $k = 0.102$, $M = 0.822$, and AoA $= 0.6$ deg is selected as a test case. The LANN wing has a supercritical airfoil section with maximum thickness-to-chord t/c ratio being equal to 12% [20]. Because of this large thickness ratio, the LANN wing could be a challenging case for ZEUS validation.

Before the unsteady computation, ZEUS will routinely perform a steady aerodynamic analysis, and this steady solution is used as the initial flow solution for unsteady aerodynamic calculation. Figure 14 shows such a steady C_p solution with and without viscous effects along six spanwise stations, $y/b = 0.2$, 0.325, 0.475, 0.65, 0.825, and 0.95, as well as their correlations with the wind-tunnel data and the CAPTSD solutions. It can be seen that the ZEUS viscous solution agrees very well with the wind-tunnel data and provides a significant improvement over the inviscid solution, especially near the transonic shock locations. It should be noted that there are two transonic shocks along the wing chord occurring at the spanwise station $y/b = 0.2$ and 0.325. These two transonic shocks are also well captured by ZEUS. Meanwhile, the CAPTSD solution fails to correctly predict the transonic shock location and strength and correlates poorly with the wind-tunnel data.

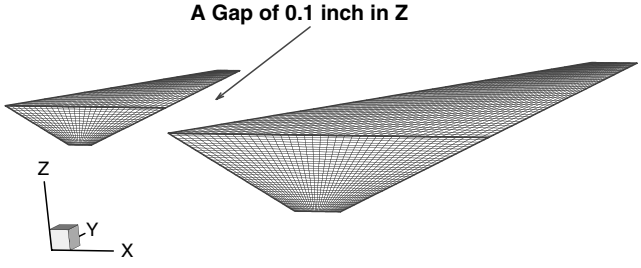

Fig. 17 Saab canard–wing configuration.

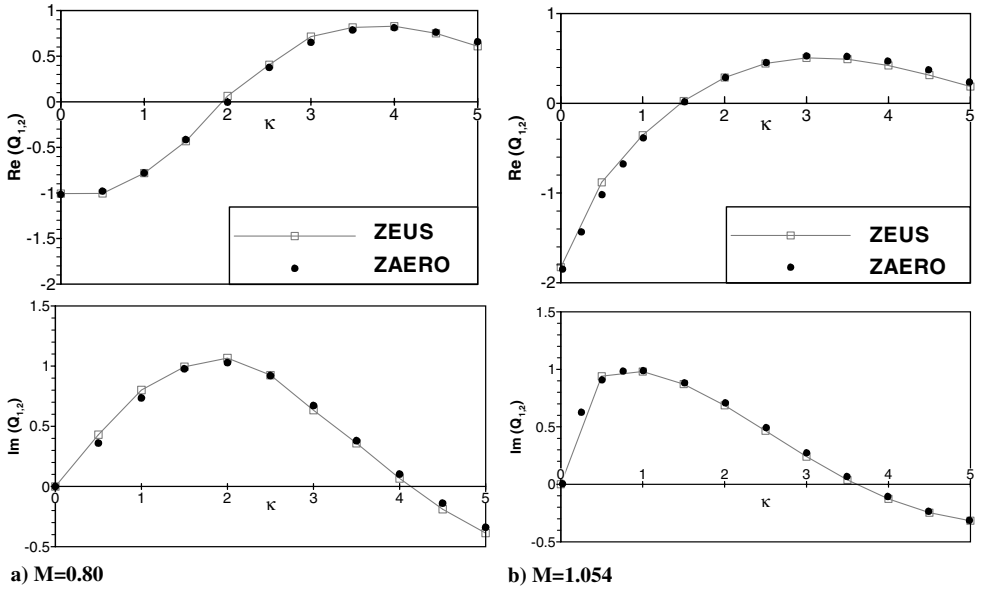

Fig. 18 Lift on the wing vs reduced frequency due to canard pitching oscillation of the Saab canard–wing model at $M = 0.8$ and 1.054.

The real part and imaginary part of the unsteady C_p on the LANN wing are shown in Figs. 15 and 16, respectively. With the boundary-layer option, the ZEUS viscous solution agrees very well with the wind-tunnel data, especially for the unsteady shock location and strength. This suggests that the unsteady shock location and strength are largely dominated by the steady shock location and strength. Therefore, if the steady shock location and strength are accurately obtained, the accuracy of the unsteady shock location and strength can be ensured, as demonstrated by the ZEUS solution on the LANN wing case. This is also evidenced by the CAPTSD solutions where its real and imaginary C_p solutions shown in Figs. 15 and 16 are totally unacceptable, as likely caused by the discrepancy of its steady solutions with the wing-tunnel data.

IX. Downwash/Wake Effects of the Saab Canard–Wing Model

The formulation of a potential flow solver is required to impose a wake boundary condition on a prescribed wake surface (fixed wake approach) or a wake shedding condition on the wing trailing edge (the free wake approach). By contrast, an Euler formulation does not need to explicitly impose such wake conditions because the vorticity imbedded in the Euler equations could self-generate wake flow shedded from a curved surface or a wing trailing edge. However, the Euler solver might suffer from the numerical dissipation if the algorithm of the solver is not properly formulated. This numerical dissipation could render the wake solution deteriorated in the downstream away from the wing trailing edge. The Saab canard–wing model [21] is an ideal case to examine the accuracy of the downwash/wake effects calculated by ZEUS. Shown in Fig. 17 is the surface mesh of a Saab canard–wing model where both the canard and wing are flat plates with a gap of 0.1 in. in the vertical direction between them. The canard is pitching about its 50% root chord while the wing remains stationary. The lift on the wing is generated mainly by the downwash/wake from the pitching canard.

Because both canard and wing are flat plates without thickness and the freestream flow is assumed to be at 0 angle of attack, there are no steady aerodynamics coupled in the unsteady aerodynamics. In addition, if the pitching amplitude of the canard is assumed to be infinitesimal, the unsteady flow becomes completely linear, for which the potential equation and the perturbed Euler equations become nearly equivalent in the Mach number range considered. In this case, the ZAERO solution (computed by the panel method) can be used to validate the ZEUS solution. Two validation cases are shown in Fig. 18, where excellent agreement of the lift on the wing at various reduced frequencies and at $M = 0.8$and 1.054 between the ZAERO solution and the ZEUS solution can be seen. This agreement clearly demonstrates the accuracy of the downwash/wake effects in terms of generalized aerodynamic forces predicted by ZEUS.

X. Flutter Boundary Prediction of the Goland Wing

The Goland wing [22] is a rectangular wing with a 4% parabolic arc airfoil section and is one of the standard benchmark cases for validating flutter solution. Figure 19 presents the flutter boundaries of the Goland wing computed by Snyder et al. [23] using the ENS3-DAE code [23] and the CAPTSD code, as well as by ZAERO and ZEUS. All those results, except that computed by ZAERO, agree well with each other and show that the flutter boundary of the Goland wing has a transonic dip around $M = 0.92$. The failure of ZAERO in capturing the transonic dip is caused by the use of the panel method to solve the linear potential equation. Beyond the flutter boundary, the aeroelastic system is unstable but the growth of the oscillating amplitude could stop if a benign nonlinearity beyond certain amplitude appears to stabilize the aeroelastic system, resulting in a limit cycle oscillation (LCO). To examine whether such a benign nonlinearity of the Goland wing could be provided by ZEUS, we selected two flow conditions, one at $M = 0.92$ and velocity $U = 600$ ft/s and the other at $M = 0.94$ and $U = 630$ ft/s (both are beyond the flutter

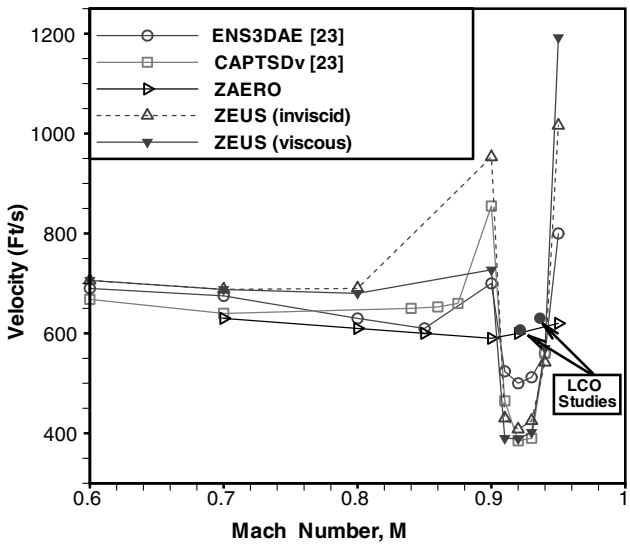

Fig. 19 Flutter boundary of the Goland wing.

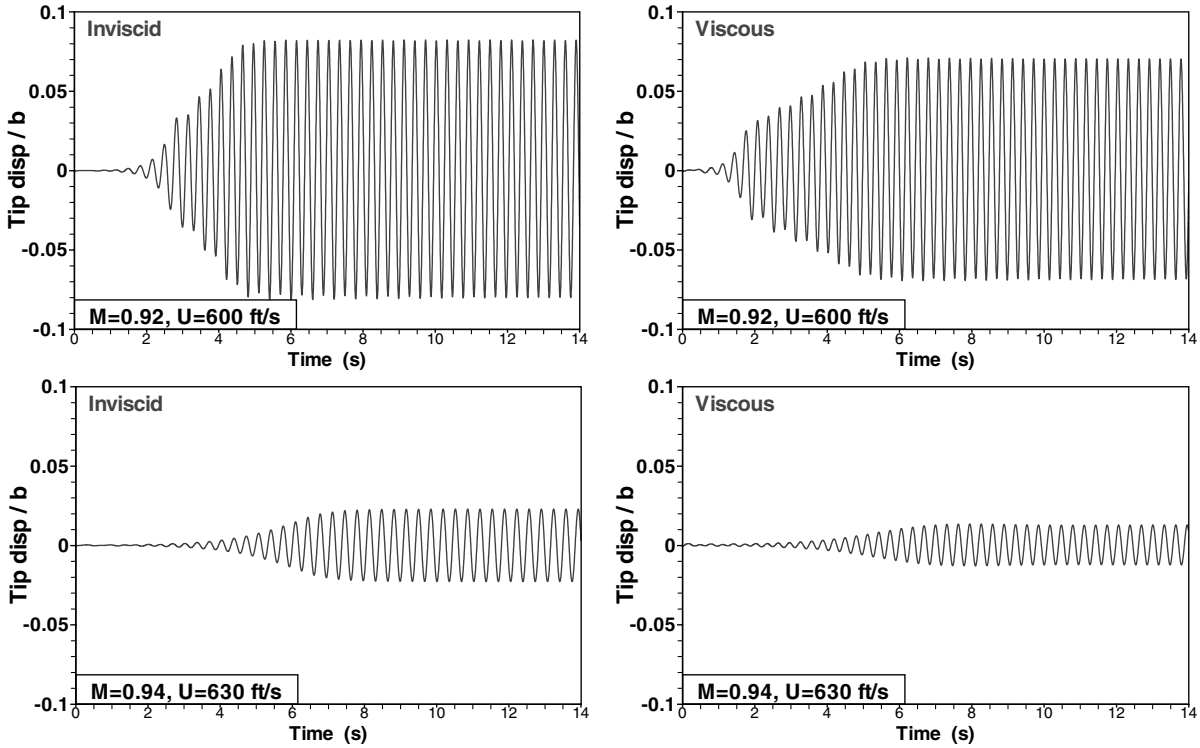

Fig. 20 LCO of the Goland wing computed by ZEUS at $M = 0.92$ and $U = 600$ ft/s and at $M = 0.94$ and $U = 630$ ft/s.

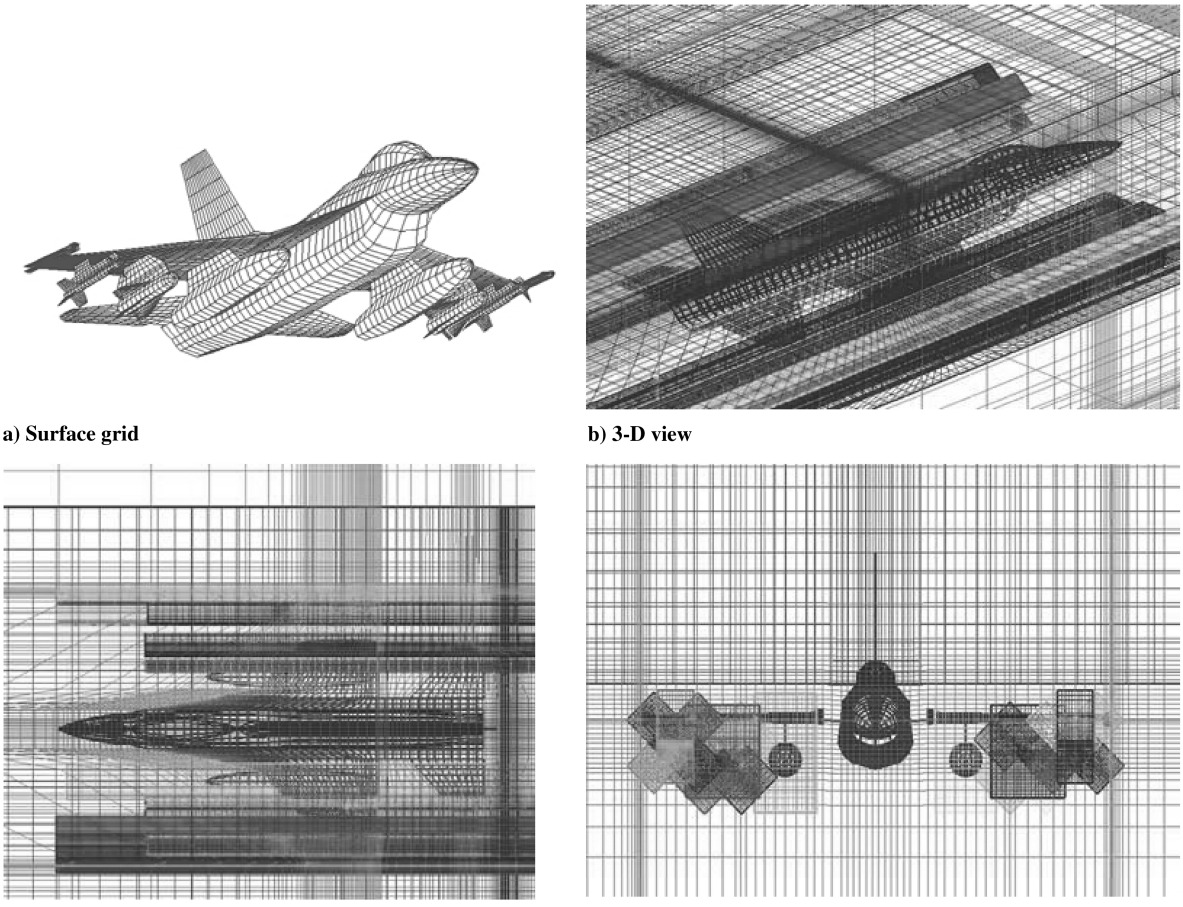

a) Surface grid **b) 3-D view**

c) X-Y view **d) Y-Z view**

Fig. 21 Twenty-four blocks of mesh to model the whole aircraft with underwing stores.

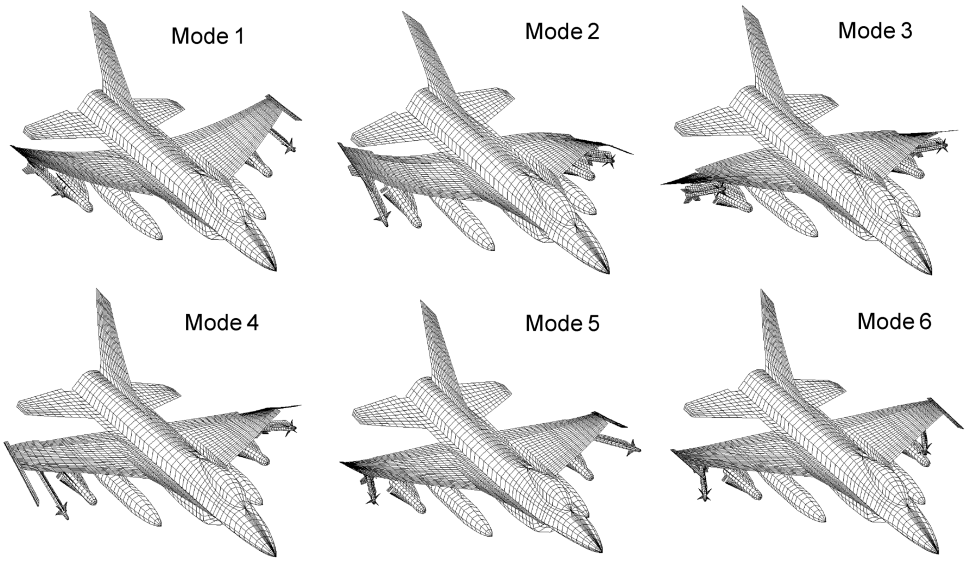

Fig. 22 Structural modes on the aerodynamic surface mesh of the typical-LCO configuration.

boundary), to compute the transient response at the wing tip. These LCO results computed by ZEUS with and without the viscous effects are shown in Fig. 20. Indeed, both ZEUS viscous and inviscid solutions show LCO at those two flow conditions, except the LCO amplitude of the viscous solution is slightly smaller than that of the inviscid solution. This suggests that the LCO of the Goland wing could be predicted by the nonlinear Euler solution with and without boundary option of ZEUS, whereas LCO persists only at a slightly reduced level in spite of the introduced viscous effects.

XI. Transient Response of a Fighter with Stores

Several current fighter aircraft with external store configurations have persistently encountered LCO problems [24,25]. It is generally believed that LCO of aircraft with stores is induced by the nonlinearity in aerodynamics or structures, or both. Ongoing LCO studies tend to focus on aerodynamic studies with transonic shock and/or shock-induced flow separation being the sole mechanism of LCO [26,27]. We believe that there might be more mechanisms involved to trigger LCO than just transonic aerodynamics [28]. In search of the mechanisms of LCO, we suggest a simulation tool that will contain the following features:

1) Its unsteady aerodynamic method must be nonlinear with captured transonic shocks.

2) Flow viscosity should be included.

3) All components of the configuration, particularly external stores, should be modeled structurally as well as aerodynamically.

4) The equation of motion should include structural nonlinearities. We propose to search for the LCO mechanism through massive computed results; hence, the simulation tool must be computationally efficient and with affordable computing resources so that computed results can be generated for massive numbers of aircraft with stores configurations at various flight conditions. ZEUS is suitable to accomplish these tasks, because of its overset mesh capability for complex configurations and being an efficient Euler solver with boundary-layer option for transonic shock and flow

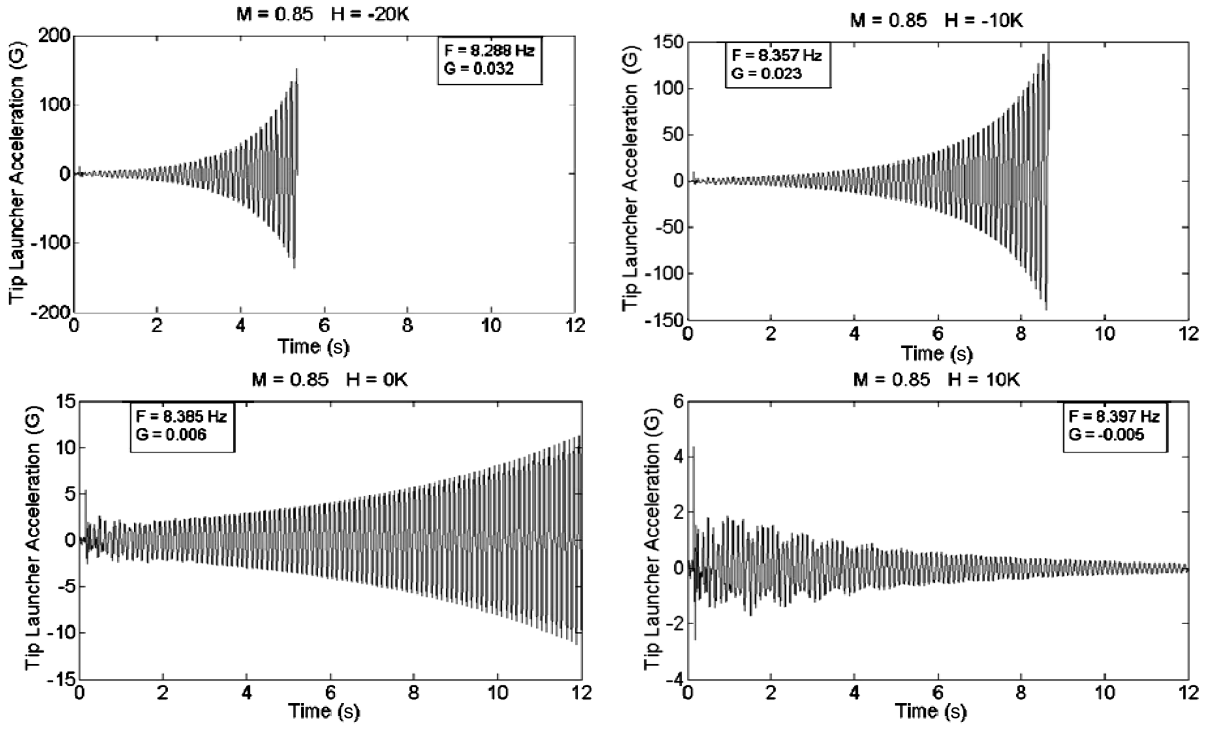

Fig. 23 Tip launcher acceleration of the typical-LCO configuration at $M = 0.85$, AoA $= 2.2$ deg, and $Re = 4.6 \times 10^6$.

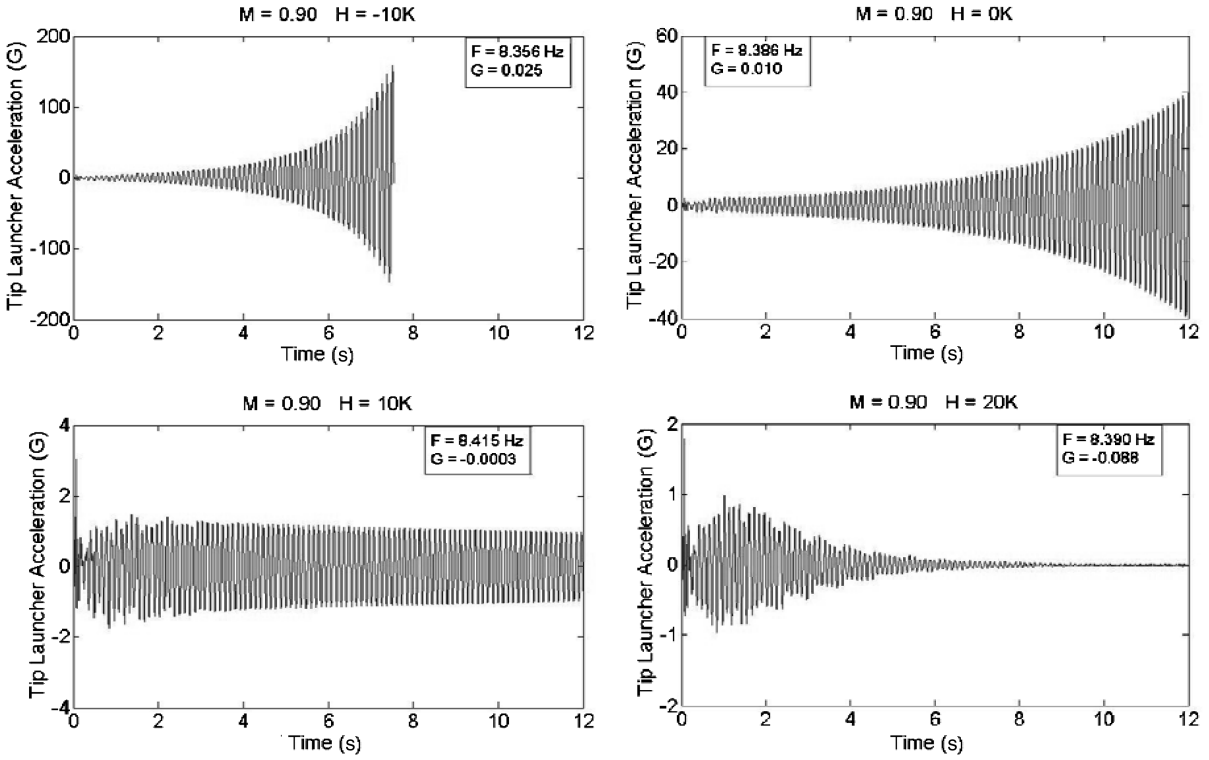

Fig. 24 Tip launcher acceleration of the typical-LCO configuration at $M = 0.90$, AoA $= 2.2$ deg, and $Re = 4.6 \times 10^6$.

viscous effects. To demonstrate ZEUS capability in this, we select an F-16 with stores configuration, called the typical-LCO configuration [25], as a test case to investigate its flutter/LCO characteristics.

The surface mesh represented by the panel model of this typical-LCO configuration is shown in Fig. 21a, where three underwing stores/missiles mounted under each side of the wing can be seen. To model such a complex configuration, we use 24 blocks of mesh whose 3-D view, X–Y view, and Y–Z view are shown in Figs. 21b–21d, respectively, rendering an overset mesh for the ZEUS computation.

To transfer the mode shapes from the structural grids to the aerodynamic grids, we employed the infinite plate spline method for the wings, tip launchers, vertical tails, and horizontal tails, the beam spline method for the fuselage and the store bodies, and the rigid body attachment method for the missile canards and fins. The resulting mode shapes on the aerodynamic surface mesh of the first six elastic modes are presented in Fig. 22.

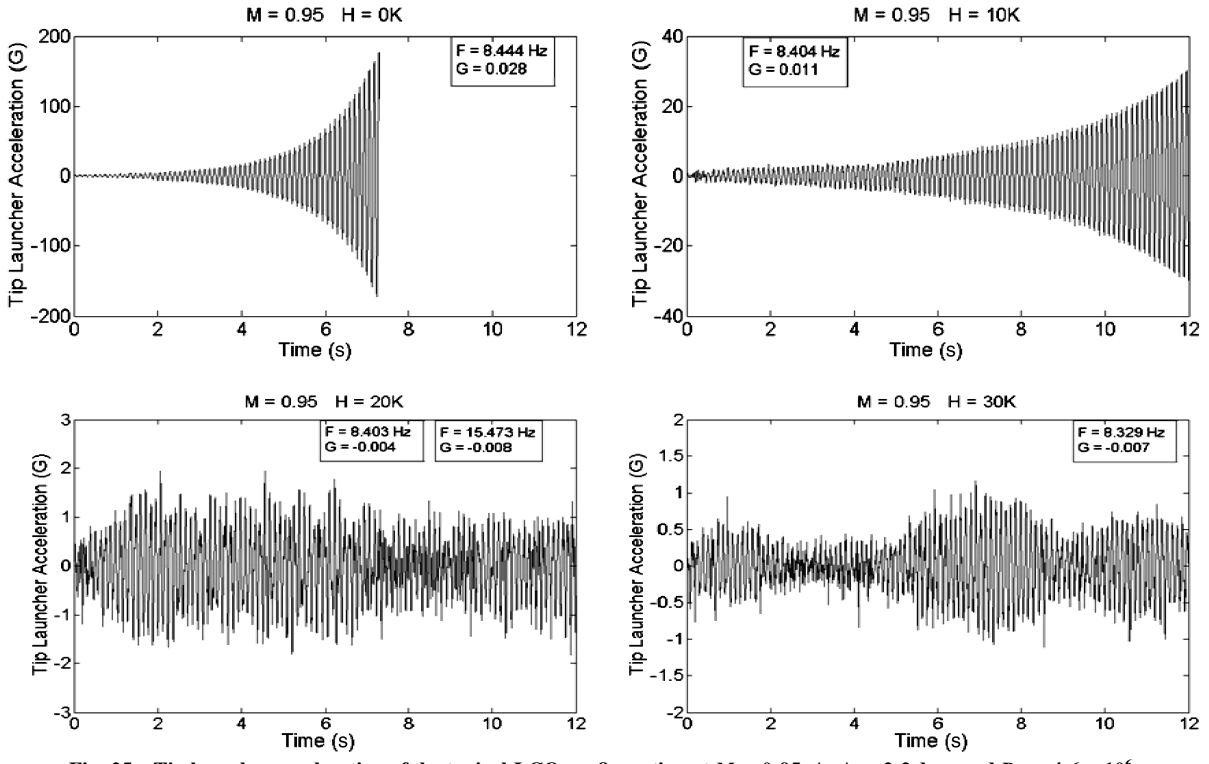

Fig. 25 Tip launcher acceleration of the typical-LCO configuration at $M = 0.95$, AoA $= 2.2$ deg, and $Re = 4.6 \times 10^6$.

Table 1 Comparison of flutter boundary between ZEUS and ZTRAN

Mach no.	Flutter speed, ft/s		Flutter frequency, Hz	
	ZEUS	ZTRAN	ZEUS	ZTRAN
$M = 0.85$	958.1	958.0	8.34	8.32
$M = 0.90$	997.8	980.3	8.36	8.37
$M = 0.95$	1012.1	1001.6	8.36	8.38

For the ZEUS transient response analysis, the angle of attack and Reynolds number are assumed to be at 2.2 deg and 4.6×10^6, respectively, and are invariant with respect to the Mach numbers and altitudes H. Three transonic Mach numbers at $M = 0.85$, 0.9, and 0.95 are selected, at which the transient response computations are performed at various altitudes. To excite the aeroelastic systems, we used the trailing-edge flaps with one-cycle antisymmetric oscillation as the initial disturbance. The use of the antisymmetric oscillation of the trailing-edge flap is under the consideration that the typical-LCO configuration is expected to have an antisymmetric LCO characteristic [25]. Before the transient response computation, a static aeroelastic analysis is performed first on the configuration; its deformed shape is based as the mean position for the follow-up dynamic aeroelastic analysis. These dynamic aeroelastic results, in terms of the transient responses at the tip launcher, are presented in Figs. 23–25, for $M = 0.85$, 0.9, and 0.95, respectively. At $M = 0.85$ and below $H = 0$ kft, divergent motions are predicted by ZEUS. A decayed motion is obtained at $H = 10$ kft, showing that the typical-LCO configuration has a flutter boundary at $M = 0.85$ between $H = 0$ and 10 kft. However, at all altitudes, no LCO is obtained at $M = 0.85$. Similarly, divergent motions below $H = 10$ kft and decay motion above $H = 20$ kft are obtained at $M = 0.9$ while no LCO is shown. At $M = 0.95$, the ZEUS results also show divergent motions below $H = 0$ kft. But above $H = 20$ k, LCOs are obtained that have a maximum acceleration of $2g$ at $H = 20$ k and $1g$ at $H = 30$ k. It is believed that this type of LCO is induced by the strong unsteady shock occurring at $M = 0.95$ and probably the shock-induced boundary-layer separation.

The frequency F and damping G of those transient responses calculated using the auto-regressive-moving-average technique are also shown in Figs. 23–25. Flutter boundary in terms of altitude at each Mach number can then be obtained by interpolating the damping values at all altitudes for zero damping. The flutter speeds and frequencies at these zero-damping conditions are presented in Table 1. In Table 1, the flutter speeds and frequencies computed by the ZTRAN method [29] are also included. The ZTRAN method is a transonic field-panel method using CFD-generated steady aerodynamic solution as the steady background flow to compute the frequency-domain unsteady aerodynamics. For these typical-LCO cases, the Navier–Stokes solution computed by the SPLITFLOW code [30] is employed to generate the steady background flow for the ZTRAN method. Good agreement between the ZEUS and ZTRAN flutter solutions can be seen in Table 1. Note that ZEUS is a time-domain approach, whereas ZTRAN is a frequency-domain approach, and such a good agreement between their flutter solutions indeed validates both codes as viable transonic unsteady aerodynamic methods for aeroelastic systems.

XII. Conclusions

A sheared-Cartesian-based Euler solver with boundary-layer option has been developed with overset mesh capability and an automated mesh-generation scheme for aeroelastic applications to complex aircraft configurations. The resulting software system of this Euler solver, called ZEUS, has been validated with various available data, including wind-tunnel data and analytical results computed by other computational methods of wings, wing–body configurations, and a fighter with external stores. Because of the built-in automated mesh-generation scheme, ZEUS does not need tedious mesh-generation efforts that are usually required by other CFD methods, thus resulting in a great savings in engineering time. This automated mesh-generation scheme can automatically generate a computational mesh for ZEUS by extending the grid lines from the surface mesh to the whole flowfield. Thus, the input of ZEUS requires only the surface mesh definition through the panel modeling of ZAERO as input, rendering ZEUS as a user-friendly, cost-effective computational tool that can be readily adopted by industry for applications to large aeroelastic systems.

References

[1] Rodden, W. P., Giesing, J. P., and Kalman, T. P., "New Method for Nonplanar Configurations," AGARD CP-80-71, Pt. 2, No. 4, 1971.

[2] ZAERO Software Package, Ver. 8.2, ZONA Technology, Scottsdale, AZ, July 2007.

[3] Guruswamy, G. P., Goorjian, P. M., Ide, H., and Miller, G. D., "Transonic Aeroelastic Analysis of the B-1 Wing," *Journal of Aircraft*, Vol. 23, No. 7, July 1986, pp. 547–553. doi:10.2514/3.45342

[4] Batina, J. T., "Efficient Algorithm for Solution of the Unsteady Transonic Small-Disturbance Equation," *Journal of Aircraft*, Vol. 25, No. 7, 1988, pp. 589–605. doi:10.2514/3.45629

[5] Edwards, J. W., "Transonic Shock Oscillations Calculated with a New Interactive Boundary Layer Coupling Method," AIAA Paper 93-0777, 1993.

[6] Batina, J. T., "Introduction of the ASP3-D Computer Program for Unsteady Aerodynamic and Aeroelastic Analyses," NASA TM-205-213909, 2005.

[7] Gao, C., Yang, S., Luo, S., Liu, F., and Schuster, D. M., "Calculation of Airfoil Flutter by an Euler Method with Approximate Boundary Conditions," *AIAA Journal*, Vol. 43, No. 2, Feb. 2005, pp. 295–305. doi:10.2514/1.5752

[8] Zhang, Z., Liu, F., and Schuster, D. M., "An Effective Euler Method on Non-Moving Carian Grids with Boundary-Layer Correction for Wing Flutter Solutions," AIAA Paper 2006-0884, 2006.

[9] Yang, S., Liu, F., Luo, S., Tsai, H. M., and Schuster, D. M., "Time-Domain Aeroelastic Simulation on Stationary Body-Conforming Grids with Small Perturbation Boundary Conditions," AIAA Paper 2004-0885, 2004.

[10] Harder, R. L., and Desmariais, R. N., "Interpolation Using Surface Splines," *AIAA Journal*, Vol. 9, No. 2, 1972, pp. 189–191. doi:10.2514/3.44330

[11] Duchon, J., "Splines Minimizing Rotation-Invariant Semi-Norms in Sobolev Spaces," *Constructive Theory of Functions of Several Variables*, edited by W. Schempp, and K. Zeller, Springer, Oberwolfach, Germany, 1976, pp. 85–100.

[12] Rodden, W. P., and Johnson, E. H., "MSC/NASTRAN Aeroelastic Analysis User's Guide," Ver. 68, Macneal–Schwender Corp., Los Angeles, 1994.

[13] Chen, P. C., "Damping Perturbation Method for Flutter Solution: The g-Method," *AIAA Journal*, Vol. 38, No. 9, Aug. 2000, pp. 1519–1524. doi:10.2514/2.1171

[14] Boope, C. W., "Computational Transonic Flow About Realistic Aircraft Configurations," AIAA Paper 78-104, 1978.

[15] Benek, J., Buning, P., and Steger, J., "A 3-D CHIMERA Grid Embedding Technique," AIAA Paper 85-1523-CP, 1985.

[16] Steger, J., Dougherty, C., and Benek, J., "A Chimera Grid Scheme," *Advances in Grid Generation*, Vol. 5, edited by K. Ghia, and U. Ghia, American Society of Mechanical Engineers, Fluids Engineering Div., Fairfield, NJ, June 1983.

[17] Thompson, F. J., Soni, B. K., and Weatherill, N. P., *Handbook of Grid Generation*, CRC Press, Boca Raton, FL, 1999.

[18] Critzos, C. C., "A Transonic Investigation of the Static Longitudinal-Stability Characteristics of a 45° Sweptback Wing-Fuselage Combination with and Without Horizontal Tail," Presented at the *National Advisory Committee for Aeronautics*, NACA Research Memo., 1 May 1956.

[19] Loving, D. L., and Estabrooks, B. B., "Transonic-Wing Investigation in the Langley 8 Foot High-Speed Tunnel at High Subsonic Mach Numbers and at a Mach Number of 1.2 Analysis of Pressure Distribution of Wing-Fuselage Configuration Having a Wing 45° Sweepback, Aspect Ratio 4, Taper Ratio 0.6, and NACA 65A006 Airfoil Section," Presented at the *National Advisory Committee for Aeronautics*, NACA Research Mem., 6 Sept. 1951.

[20] Malone, J. B., and Ruo, S. Y., "LANN Wing Test Program: Acquisition and Application of Unsteady Transonic Data for Evaluation of Three-Dimensional Computational Methods," U.S. Air Force Wright

Aeronautical Labs. TR-83-6006, Feb. 1983.
[21] Johnson, E. H., Rodden, W. P., Chen, P. C., and Liu, D. D., "Comment on 'Canard-Wing Interaction in Unsteady Supersonic Flow'," *Journal of Aircraft*, Vol. 29, No. 4, July–Aug. 1992, p. 744. doi:10.2514/3.46240
[22] Schuster, D. M., Beran, P. S., and Huttsell, L. J., "Application of the ENS3-DAE Euler/Navier–Stokes Aeroelastic Method," AGARD Rept. 822, 1997.
[23] Snyder, R. D., Scott, J. N., Khot, P. S., and Zweber, J. V., "Prediction of Store-Induced Limit-Cycle Oscillations Using Euler and Navier–Stokes Fluid Dynamics," AIAA Paper 2003-1727, 2003.
[24] Denegri, C. M., Jr., "Limit Cycle Oscillation Flight Test Results of a Fighter with External Stores," *Journal of Aircraft*, Vol. 37, No. 5, Sept.–Oct. 2000, pp. 761–769. doi:10.2514/2.2696
[25] Denegri, C. M., Jr., Dubben, J. A., and Maxwell, D. L., "In-Flight Wing Deformation Characteristics During Limit Cycle Oscillations," *Journal of Aircraft*, Vol. 42, No. 6, 2005, pp. 1645–1652. doi:10.2514/1.21249
[26] Cunningham, A. M., Jr., and Meijier, J. J., "Semi-Empirical Unsteady Aerodynamics for Modeling Aircraft Limit Cycle Oscillations and Other Non-Linear Aeroelastic Problems," Confederation of European Aerospace Societies, 1995, pp. 74.1–74.14.
[27] Meijier, J. J., and Cunningham, A.M., Jr., "Outline and Applications of a Semi-Empirical Method for Prediction Transonic Limit Cycle Oscillation Characteristics of Fighter Aircraft," Confederation of European Aerospace Societies, 1995, pp. 75.1–75.19.
[28] Chen, P. C., Sarhaddi, D., and Liu, D. D., "Limit Cycle Oscillation Studies of a Fighter with External Stores," AIAA Paper 98-1867, 1998.
[29] Chen, P. C., Gao, X. W., and Tang, L., "Overset Field-Panel Method for Unsteady Transonic Aerodynamic Influence Coefficient Matrix Generation," *AIAA Journal*, Vol. 42, No. 9, Sept. 2004, pp. 1775–1787. doi:10.2514/1.4390
[30] Karman, S. L., Jr., "SPLITFLOW: A 3-D Unstructured Cartesian/Prismatic Grid CFD Code for Complex Geometries," AIAA Paper 1995-0343, 1995.